

Chapter 3

Very High-Frequency Digital Ultrasound: Artemis 2 Scanning in LASIK

DAN Z. REINSTEIN, MD, MA (CANTAB), FRCSC AND RONALD H. SILVERMAN, PHD

INTRODUCTION: THE ARTEMIS VERY HIGH-FREQUENCY DIGITAL ULTRASOUND ARC B-SCANNER

Digital signal processing of ultrasound backscatter was pioneered by Coleman and coworkers at the Bio-Acoustic Research Facility in the Department of Ophthalmology of Cornell University, New York, NY in the 1980s. In the early 90s we began integration of very high-frequency (VHF) probes originally designed for quality control in the metallurgical industry into the Cornell University three-dimensional (3-D) ultrasound scanning prototype. Pavlin, Sherar, and Foster at the University of Toronto also produced a VHF ultrasound scanner, but based only on conventional analog signal processing.¹ The Toronto prototype became a commercial unit called the Ultrasound Biomicroscope (UBM) manufactured by Humphrey Zeiss (Dublin, Calif). The Cornell prototype and patents were assigned to Ultralink LLC (St. Petersburg, Fla). They have subsequently developed and commercialized the first VHF digital ultrasound arc B-scanner.

The Artemis (Figure 3-1) was created in conjunction with Cornell University researchers Reinstein, Silverman, Coleman, and colleagues and is based on their intellectual property and patents from the Bio-Acoustic Research Facility in the Department of Ophthalmology of the Weill Medical College of Cornell University. Reinstein and Silverman focused on anterior segment refractive surgical applications, while Coleman, Silverman, and colleagues continued to apply the technology to the study of accommodation, ocular tumors and imaging, and analysis of the posterior pole.^{2,3}

The Artemis was designed to help ophthalmologists in all disciplines, but particularly to improve anatomical diagnosis for surgical planning and postoperative diagnostic monitoring in refractive, cataract, and presbyopic sur-

gery. The Artemis' primary functions are to provide very high resolution ultrasound B-scan imaging of the anterior and posterior segment, high-precision 3-D mapping of individual corneal layers, 3-D mapping of anterior segment dimensions, and axial length by a combined additional immersion A-scan probe. The Artemis is designed to scan in an arc of adjustable radius, thus following the curved surfaces of either the cornea, the iris plane, or the globe and enabling wide segments (up to 15 mm) to be imaged within one scan sweep.

The resolution of the Artemis, when set to scan cornea, is sufficient to distinguish individual corneal layers such as the epithelium, stromal component of the flap, residual stromal bed, and others, all in 3-D, thanks to multimeridional scanning. The Artemis VHF digital ultrasound technology is able to consistently detect internal corneal lamellar interfaces, such as the keratectomy track, because of the permanent "mechanical" interface present, even years after surgery, and despite total optical transparency. Analog UBM is not able to image the interface consistently because analog processing does not produce a high enough signal-to-noise ratio between interface echo complex and the surrounding tissue. OCT has been shown to be capable of detecting the interface in laser in-situ keratomileusis (LASIK) in the early postoperative period, but this ability diminishes with time as edema subsides in the cornea and the optical properties of the corneal lamellar interface homogenize. We have scanned former nonfreeze keratomileusis patients more than 10 years after surgery and have been able to clearly delineate, end-to-end, the lamellar interface.

In 1993, we reported the first confirmed measurement of the epithelium of the cornea in vivo, using VHF ultrasound, demonstrating that acoustic interfaces that were being detected were indeed located spatially at the epithelial surface and at the interface between epithelial cells and the surface of Bowman's layer.⁴ We also reported the first high-precision 3-D thickness mapping of the corneal

epithelium and flap.⁵ This system, acquiring a series of parallel, rectilinear B-scans, was capable of mapping the epithelial layer thickness within the central 3- to 4-mm area. By using digital signal processing techniques (the I-scan), a 2.0- μm reproducibility for epithelial thickness measurements was obtained.⁶ The I-scan is an A-scan-like trace produced by digital processing of the stored radio frequency ultrasonic data. The trace represents the instantaneous energy intensity with time as opposed to the average amplitude as is represented by the conventionally employed A-scan. Previous studies demonstrated that the I-scan more than doubles the measurement precision afforded by the analog A-scan process.⁶ We further improved epithelial thickness measurement precision to 1.3 μm by increasing the fidelity of the digitized signal.⁷ Measurement precision within the cornea in LASIK has been formally tested and published. The axial measurement precision within 9-mm-wide corneal scans is approximately 1 μm .⁸ When scans are expanded to include the entire anterior segment (15-mm width), the axial precision remains similar, while the lateral precision for measuring angle-to-angle is 0.15 mm, and from sulcus-to-sulcus, 0.20 mm.⁹ Axial measurement precision will be higher than lateral measurement precision because axial measurements are made from analysis of data within scan lines (pulse-echo axis), while lateral measurements are made from analysis of data between adjacent scan lines.

This VHF digital ultrasound system has been used to characterize central epithelial lenticular anatomy and to demonstrate that the power of the epithelium is not constant from eye to eye.¹⁰ We have also examined the shape of Bowman's layer,¹¹ the measurement of anterior corneal scars for planning therapeutic keratectomy,¹²⁻¹⁴ the quantitative analysis of corneal scarring (haze) after PRK,¹⁵ and the measurement of the depth of radial keratotomy incisions.¹⁶ In 1999, we were the first to publish an analysis of epithelial and stromal changes after lamellar corneal surgery demonstrating significant epithelial changes after uncomplicated LASIK and the masking of stromal surface irregularities that were producing optical complications.⁷ This chapter will focus on this application.

ARTEMIS TECHNOLOGY

Details of the scanning and signal processing technology have been described comprehensively elsewhere.^{4,8,12,17} Briefly a broad-band 50 MHz VHF ultrasound transducer (bandwidth approximately 10 to 60 MHz) is swept by a reverse arc high-precision mechanism to acquire B-scans as arcs that follow the surface contour of anterior or posterior segment structures of interest. The Artemis possesses a unique scan-arc adjustment mecha-



Figure 3-1. Artemis 2: VHF digital ultrasound 50 MHz 3-D arc B-scan (Ultralink, LLC).

nism to enable maximum perpendicularity (and signal-to-noise ratio) to be obtained for scanning any of the different curvatures within the globe (ie, cornea, iris plane, retina). Ultrasound data are first digitized and stored. The digitized ultrasound data are then transformed using Cornell digital signal processing technology. Digital signal processing significantly reduces noise and enhances signal-to-noise ratio. We have demonstrated that using digital signal processing on 50 MHz ultrasound data doubles resolution and increases measurement precision by a factor of three when compared to conventional analog processing of the same VHF data.⁶ Scanners produced by Paradigm (UBM), OTI (35MHz), and others employ only analog ultrasound processing.

As a result of a unique, coaxial, simultaneous video image capture at each scan position (Figure 3-2), a correlation of measurements made from the ultrasound scans can be formed into visible ocular landmarks (such as the corneal reflex) and enables accurate 3-D reconstructions made from multiple meridional scans and the production of corneal mapping. Simultaneous optical and ultrasound imaging also enables the anterior segment sulcus-to-sulcus distance to be determined in a verified plane, such as the visual axis for surgical planning in phakic IOL surgery. For the first time, it also enables localization of the optimum implantation site for devices such as scleral expansion bands, which need to be positioned based on internal (invisible) landmarks. The Artemis possesses a software application that will give the surgeon external landmarks identifiable under the operating microscope that identify the location of lens equator based on a caliper measurement from the corneal reflex (Figure 3-3).

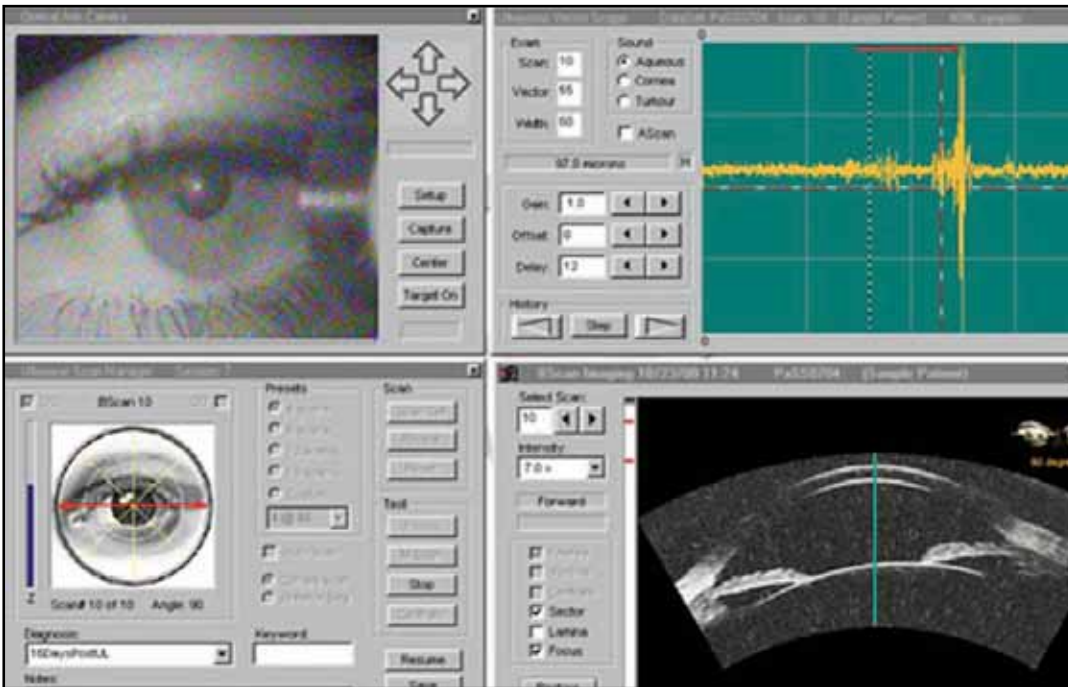


Figure 3-2. Artemis advanced control display panel. The upper left quadrant shows an infrared real-time video image of the eye being scanned in which eye position can be verified and monitored during scanning. The lower left panel is used for scan motion control, while the upper right panel displays the raw ultrasound echo data. In this screen-shot, the lower right anterior segment scan was known to have been taken in the horizontal plane when the eye was fixating on a light source co-axial with an alignment beam that is centered on the corneal vertex (corneal reflex visible). The patient’s angle kappa produces a geometrical tilt of the anterior segment compared to the visual axis (green line). The corneal reflex is an excellent landmark for correlating scans taken before and after anatomy by subtraction imaging.

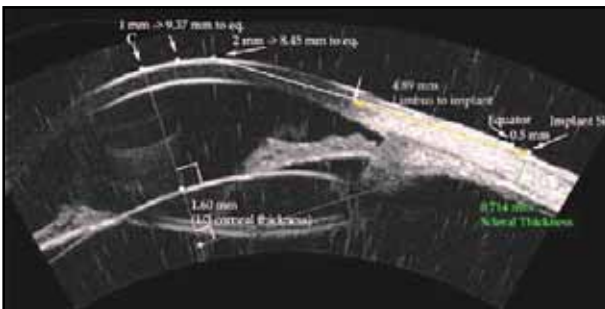


Figure 3-3. Annotated arc B-scan ultrasound image showing all measurements required for the accurate implantation of a scleral expansion band. The intersection of the cornea with the line-of-sight is indicated by arrow and “C”. The lens equator plane is localized based on the ultrasound image, and the eternal intersection of this plane at the scleral surface is localized. The distance from C to the equatorial plane is identified for exact localization of the scleral implant to achieve maximum effect. The thickness of the sclera is provided in order to maximize depth without intraoperative exposure of the choroid.

While Artemis scanning is a noncontact test, it does require an ultrasonic standoff medium, and thus provides the advantages of immersion scanning. The Artemis 2 was designed specifically to enable quick setup of this immersion scanning by a novel (patented) reverse-immersion technique. The patient sits and positions his or her chin on a three-point forehead and chin rest while placing the eye into a soft rimmed eye-cup akin to a swimming goggle (Figure 3-4). The sterile coupling fluid fills the compartment in front of the eye and the scanning is performed via an ultrasonically transparent (sterile) membrane, without the need for a speculum. Thus, there is no contact by the scanner probe with the eye. Performing a 3-D scan set with the Artemis requires 2 to 3 minutes for each eye.



Figure 3-4. Patient demonstrating the simple set-up of the reverse immersion scanning system. The patient achieves head stabilization by resting against a tripod of support points: an adjustable chin rest and two adjustable forehead rests. The eye rests comfortably in a sterile, cushioned eye-seal that produces a separate sterile compartment for the eye from the fluid-filled scanner mechanism compartment.

Clinical Utility

Two-Dimensional B-Scan Imaging

Figure 3-5 demonstrates an arc B-scan taken along the horizontal plane of the cornea of a patient 4 months after LASIK. The interfaces of saline-epithelium (E), epithelium-Bowman's (B), the keratectomy interface (K), and the posterior surface (endothelial-aqueous) (P) are clearly visualized along the 9-mm chord-length of the B-scan preoperatively. The keratectomy interface can be seen with an entrance track nasally (S), coursing temporally to a stop at the hinge (H). Magnification of the keratome entrance position shows that the flap was not fully distended and Bowman's was not fully apposed, potentially inducing astigmatism and/or increasing the risk of epithelial ingrowth. The interface track has a small irregularity (I) (magnified insert), perhaps caused by a patient squeeze during passage of the keratome. The flap can be seen to be thicker temporally and thinner (T) nasally.

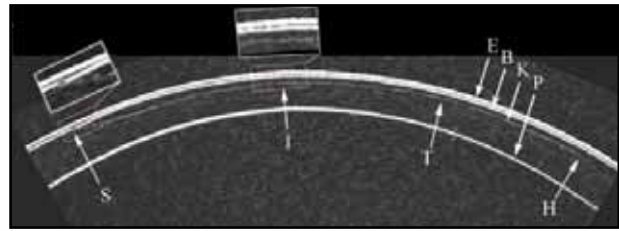


Figure 3-5. Horizontal B-scan through the visual axis of a cornea 4 months post-LASIK. The interface is clearly visualized throughout the length of the keratectomy. See text for annotations.

Three-Dimensional Reinstein C12 Diagnostic Display

This display configuration and format forms the mainstay and state-of-the-art in anatomical diagnosis after LASIK. Figure 3-6 shows such a display created from scans of the right cornea of a patient scanned before and 6 months after LASIK for myopia of $-4.75 -0.25 \times 55$. Uncorrected visual acuity was 20/16 with a residual subjective manifest refraction of plano. Videokeratographic examination showed the customary central flattening with a small surface with-the-rule astigmatism. The lamellar interface was only faintly detectable in places by slit-lamp examination.

This display of 12 pachymetric maps was designed as a standardized layered pachymetric summary of corneal anatomical changes following LASIK. We have chosen to name this presentation a Reinstein C12 diagnostic display, for it consists of 12 corneal pachymetric topographical maps of the same cornea before and after LASIK. Each map depicts the local thickness of a given corneal layer represented on a color scale in μm . The Reinstein C12 display was designed as a layout of map groupings by time, anatomic depth, and calculation. Columns 1 and 2 depict maps pre- and postoperatively. Within these two columns, the rows represent depth within the cornea. Thus, the first column depicts the thickness profiles of the preoperative corneal epithelium (Figure 3-6, map 1), full stroma (Figure 3-6, map 2), and full cornea (Figure 3-6, map 3), respectively. The second column demonstrates the postoperative thickness profiles of the corneal epithelium (Figure 3-6, map 4), stroma (Figure 3-6, map 5), and full cornea (Figure 3-6, map 6). Epithelium, full stroma, and full cornea color scales are identical for pre- and postoperative stages to allow direct color (thickness) comparison. The third column consists of calculated maps representing topographical epithelial change (Figure 3-6, map 7) (derived by subtraction of the preoperative epithelial map from postoperative epithelial map), the stromal change (Figure 3-6, map 8) (derived by subtraction of the postoperative from preoperative stromal map), and the

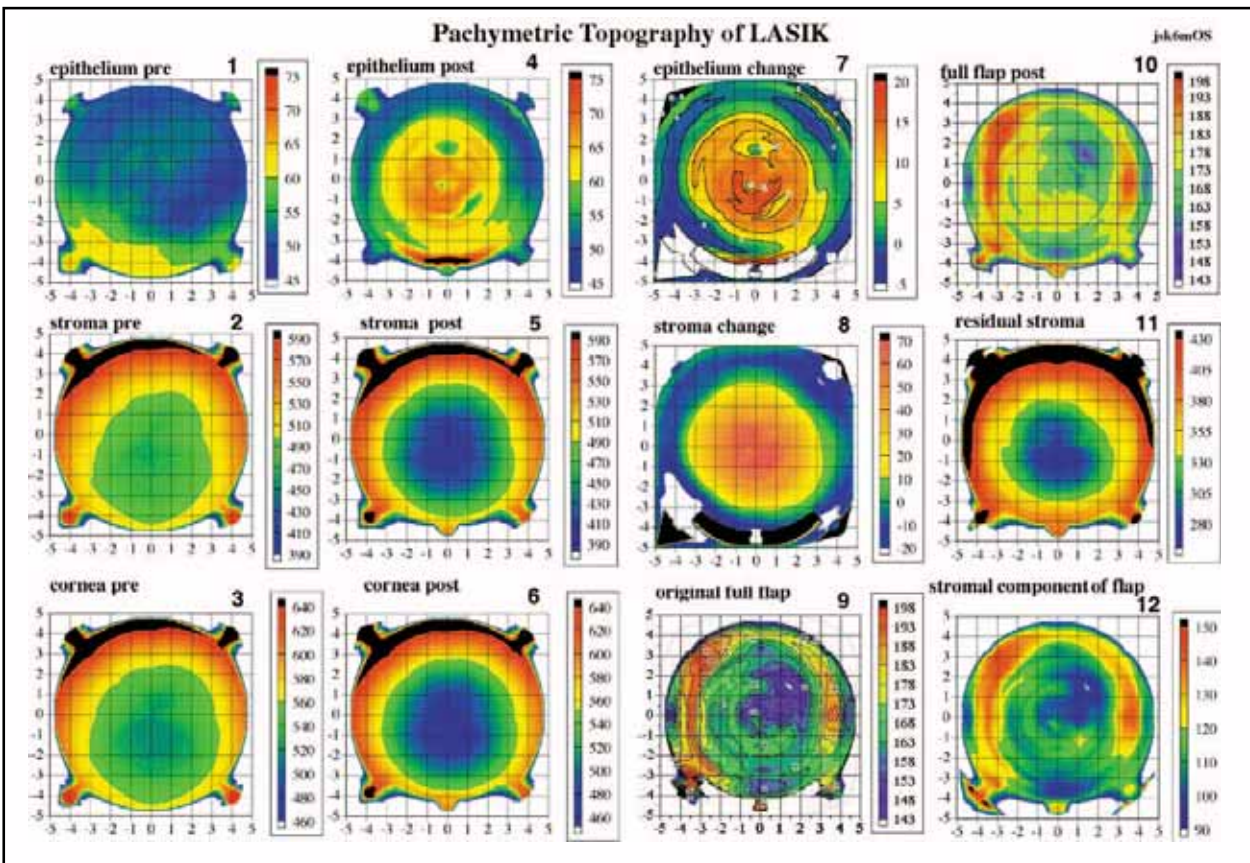


Figure 3-6. Reinstein “C12” display of the cornea of a patient pre-LASIK and 6 months post-LASIK OS. All 12 maps are pachymetric representations of particular corneal layers depicted on a color scale in microns. The pre-operative epithelial (1), stromal (2), and full corneal (3) thickness maps appear in the first column. To the right of each of these maps (column two) is the post-LASIK pachymetric maps of epithelium (4), stroma (5), and full cornea (6) on identical color scales for direct comparison to preop. The third column depicts calculated maps only. The calculated epithelial change map (7, third column, first row) is derived in point-by-point subtraction of the preoperative from the postoperative epithelial pachymetric map. Thus, the epithelial change map shows on a color scale the number of microns increase due to surgery. Note that the pattern of epithelial thickness change is such that it is greatest centrally, with a decrease in a symmetrical centrifugal fashion thus producing an increase in outer curvature of the postoperative cornea. Note that the area of epithelial thickening is confined to the ablation zone or the zone of surgical corneal flattening. The calculated stromal change map (8, third column, second row) is derived in point-by-point subtraction of the postoperative from the preoperative stromal pachymetric map. Thus the stromal change map shows on a color scale the number of stromal microns decrease due to surgery in a topographic fashion and hence represents the ablation volume of tissue. The calculated map of the “original flap” (9, third column, third row) is derived by addition of the preoperative epithelial thickness profile (1) to the postoperative “stromal component of the flap” (12, fourth column, third row). It is necessary to perform a temporally displaced addition of epithelial and stromal components of the flap separately because of the epithelial changes present post-LASIK, leading to a flap anatomy post-LASIK (10, fourth column, first row) that is different from that at the time of creation by the keratome. Finally, the pachymetric topography of the “residual stromal layer” comprising all stroma beneath and around the flap is shown in map 11 (fourth column, second row). This map can be critically important in the determination of adequacy of the stromal bed for further LASIK enhancement surgery under the flap in that the thinnest point is not always located centrally and may be missed by any form of intraoperative single-point measurement of the bed. Thus the “C12” display is set out to be read by temporal grouping (columns) or anatomical grouping (rows). See text for further descriptive analysis.

(calculated) original flap produced at the time of surgery (ie, a Reinstein flap profile) (Figure 3-6, map 9).¹⁸ The Reinstein flap profile is calculated by adding the stromal component of the flap (Figure 3-6, map 12) to the preoperative epithelial thickness. The fourth column represents postoperative corneal layers: the thickness profile of the flap at 6 months (including epithelial changes) (Figure 3-6, map 10), the 3-D thickness profile of the residual stromal layer (stroma excluding the flap), and the postoperative stromal component of the flap (Figure 3-6, map 12).

The profile map of the preoperative epithelium oculus sinister (OS) was approximately 9.25 mm in diameter (Figure 3-6, map 1). The epithelial change map (Figure 3-6, map 7) shows the pattern of epithelial thickening and thinning. The epithelium thickened between 15 and 20 μm centrally, with a concentric decrease in thickening progressing toward the 7.5-mm diameter zone. It is interesting to note that there was circumferential epithelial thinning after LASIK within a 1-mm annulus at the 8-mm diameter zone. We also note in this case that the pattern of epithelial change increased anterior corneal power (greater tissue addition centrally), but the patient had a plano refraction postoperatively. This indicates that the optical power shift produced by the epithelium in this case was exactly as expected by the nomogram setting used.

The stromal change map (see Figure 3-6) shows a well-centered difference about the center (0,0 coordinate) of the cornea. The difference in stromal thickness prior to surgery is 70 μm centrally, decreasing to zero at the 7.5-mm diameter zone. Thus, the zone depicted on the color scale from green to red represents the effective volume of tissue change in the cornea (the predicted central ablation depth by the Nidek EC5000 [Nidek, Gamagori, Japan] readout was 73 μm for a 6.5-mm optical zone, transition to 7.5 mm). Within the peripheral 8- to 9-mm zone there is annular stromal thickening of between 10 and 20 μm . We were the first to publish this finding,⁸ and Roberts has proposed a mechanism to account for it.¹⁹ It is also interesting to note that this annulus of stromal thickening coincides with the annulus of epithelial thinning described above consistent with the Reinstein's law of epithelial compensation (see below).

Examination of the anatomy of the calculated original flap (Figure 3-6, map 9) by the Moria LSK-One keratome (predicted mean 160 μm) reveals a central thickness of 158 μm . Within the 4-mm diameter zone, the flap thickness was generally homogeneous between 160 and 165 μm although irregularity is evident. Note that direct measurement of the flap thickness at 6 months (Figure 3-6, map 10) would not provide an accurate description of the flap anatomy at the time of creation due to the epithelial thickness changes present after LASIK. The stromal component of the flap (Figure 3-6, map 12) can be seen to

possess a thickness profile of approximately 110 to 120 μm within the central 6-mm diameter zone, except for the quadrant superotemporally within the 4-mm diameter zone, where this is decreased to approximately 95 μm . This area may have been thinner due to the presence of thicker epithelium preoperatively in the corresponding quadrant, and the passage of the keratome parallel to the surface of the cornea during applanation by the keratome head.

The 3-D thickness profile of the residual stromal layer (Figure 3-6, map 11) shows a thinnest point of 280 μm approximately 1 mm inferior to the center of the cornea. This is an example of why intraoperative hand-held ultrasound residual stromal pachymetry can be unsafe. Lateral position variations of only a few hundred microns could completely alter the course of an ablation by providing a residual stromal thickness that is not the minimum.

PREOPERATIVE ASSESSMENT

Corneal Thickness Profile: Minimum Thickness and Screening for Keratoconus

The importance of accurate preoperative corneal thickness profile determination is now generally accepted as an aid in the determination of candidacy for safe LASIK with avoidance of ectasia.²⁰ Concentricity of the thickness profile about the corneal center is also a contributor in screening for keratoconus. Because of the significant, added expense to the patient for Artemis scanning, at present we offer to but do not routinely use this preoperatively in every patient. Current indications for Artemis scanning in our practice include a greater than 15- μm discrepancy between Orbscan (Bausch & Lomb Surgical, Irvine, Calif) and hand-held ultrasound pachymetry and a predicted residual stromal thickness of less than 300- μm based on whichever is the thinnest of Orbscan or hand-held ultrasound pachymetry.

The accuracy of measurement is defined as the concordance between the measured and the true value. A theoretical error analysis to estimate the accuracy of Artemis pachymetry has been published.⁸ The accuracy of Artemis thickness measurements within the cornea was found to be at worst $\pm .8\%$. This means that the 95% confidence interval for concordance between the measured and the true value is expected to be within $\pm 5 \mu\text{m}$ for corneal thickness measurements (mean thickness 515 μm by VHF digital ultrasound).⁶

Optical methodology for the determination of corneal back surface shape and hence 3-D corneal thickness mapping, although possessing the convenience of in-air data acquisition, suffers from variable accuracy²¹⁻²³ almost cer-

tainly due to a large extent to the variable optical properties of the cornea before and after corneal refractive surgery.²⁴ Variations in refractive index of the cornea probably also exist between normal, unoperated individuals. We conducted a central corneal thickness study in which we compared measurements in 52 unoperated eyes obtained by Orbscan with those from VHF digital ultrasound scanning. Orbscan was found to be approximately four times less accurate. The variance was $\pm 25 \mu\text{m}$ (SD) greater in the Orbscan group compared to the VHF digital ultrasound group (95% confidence interval $\pm 35 \mu\text{m}$), amounting to a loss of accuracy by another 7%.

POSTOPERATIVE ASSESSMENT WITH ARTEMIS TECHNOLOGY: TRUE DIAGNOSIS AFTER LASIK AND OPTIMAL TREATMENT PLANNING

While LASIK and PRK are already relatively safe procedures today, we are constantly striving to make them even safer. We need to prevent complications, and when these do occur we need methods for correcting them and restoring visual function. In keeping with basic principles of surgery, accurate imaging and biometry will be the cornerstone of these goals, since accurate diagnosis enables optimal treatment planning.

Surface topography has been the mainstay of diagnostic testing in complicated LASIK. Recently, the introduction of aberrometry has greatly enhanced our diagnostic capabilities in understanding in a quantitative way how irregular astigmatism and other shape irregularities produce visual complaints. However, neither the understanding of the optical defect or the surface shape of the cornea will necessarily provide a diagnosis for the cause of the problem.⁷ The anatomical cause of a surface abnormality may only be understood at an internal corneal level (eg, irregularities in the flap vs the stromal bed). With burgeoning surgical rates of PRK and LASIK worldwide, it is becoming increasingly evident that there is a distinct need for a method of determining the layered anatomy of the changes induced. Without an accurate anatomical diagnosis, topography or wavefront-guided treatments may lead to a suboptimal treatment plan.

The development of VHF digital ultrasound corneal scanning technology was first reported in 1991 in which digital signal processing was used to identify and analyze the epithelium and scar layers formed in an experimental rabbit model.¹² In 1993, we reported the first confirmed measurement of the epithelium of the cornea *in vivo*, demonstrating that the acoustic interface detected within

the intact cornea was localized spatially at the interface between epithelial cells and the surface of Bowman's layer.⁴ This system, acquiring a series of parallel, rectilinear B-scans, was further developed to enable mapping the thickness profile of the epithelium⁵ as well as the lamellar flap within the central 3- to 4-mm area. By using digital signal processing techniques (the I-scan),⁶ a 2.0- μm reproducibility for epithelial thickness measurements was obtained.⁶ Subsequently, by increasing the fidelity of the digitized signal, flap thickness measurement precision was further improved to 1.3 μm , with epithelial and corneal measurements attaining a reproducibility of under 1 μm .⁸ In clinical application, analysis of epithelial and stromal changes after lamellar corneal surgery has demonstrated significant epithelial changes after uncomplicated LASIK and the masking of stromal surface irregularities that were producing optical complications.⁷

The importance of epithelial changes in corneal refractive surgery has probably been underestimated. Significant changes in epithelial thickness profiles in both PRK^{25,26} and LASIK²⁷⁻²⁹ have been demonstrated and implicated in regression as well as the inaccuracy of topographically guided excimer laser ablation.⁷ The curvature of Bowman's layer in the center of the normal cornea is on average greater than that of the epithelial surface.¹¹ As the refractive index of epithelium and stroma are sufficiently different (1.401 vs 1.377),³⁰ the epithelial-stromal interface constitutes an important refractive interface within the cornea, with a mean power contribution estimated at approximately -3.60 diopters (D).¹¹ Thus, unpredicted changes in the epithelial lenticule after surgery will result in unplanned refractive shifts. This is one of the reasons why current ablation depths and profiles ("nomograms") differ from theoretical ablation profiles; they incorporate the average change of epithelial power for a given level of stromal surface flattening (level of myopia treated). Thus, the understanding of epithelial dynamics and their patterns begin to unfold,^{28,29} and these factors may potentially be used to improve the accuracy of corneal refractive outcomes.

Artemis scanning will significantly contribute to LASIK accuracy and safety. Accuracy in LASIK translates to the chances of an eye achieving target refraction. Safety relates to achieving this target without loss of best spectacle-corrected visual acuity (BSCVA) or other visual disturbance.

Ectasia is one of the most devastating potential consequences of LASIK and it behooves us to prevent it from happening in every possible way. The thickness of the flap determines at what level stromal tissue removal commences, and hence is directly related to the amount of stromal tissue remaining in the posterior cornea under the flap after surgery. The thinner the flap the more difficult it is to handle surgically; however, the thicker the flap,

Table 3-1
REINSTEIN CLASSIFICATION OF FLAP MICROFOLDS IN LASIK

<i>Type</i>	<i>Anatomic Location</i>	<i>Loss of BSCVA</i>	<i>Fluorescein Pooling</i>	<i>Clinical Findings</i>	<i>Anatomical Basis</i>	<i>Management</i>
Corrugation	Stroma			Gross folds, differential pooling of gutters, mixed-cylinder	Flap slip	Flap repositioning
True microfolds	Bowman's			Grooves in Bowman's	Grooves in Bowman's	Flap repositioning and microfold distention
Bowman's	Bowman's		∅	Gray lines no groove	Fractures in Bowman's	Observe only

These anatomical disturbances often change astigmatism and produce loss of BSCVA. Anatomical localization within the flap is important in designating the optimal management plan.

the less tissue remains for the correction of ametropia by LASIK. Below are some clinical examples demonstrating the importance of distinguishing biomechanical from epithelial components of ametropia after an initial treatment.

Despite all the advances in corneal topography and ocular wavefront measurement, it is not always possible to diagnose the cause of subjective visual complaints by these means alone.⁷ This is due to the fact that internal corneal refractive interfaces (such as the epithelial-stromal interface) are not being measured independently. In fact, topography is often not, strictly speaking, a diagnostic test but rather a descriptive one. For the diagnosis and correction of complications, identifying the anatomical cause of a corneal surface abnormality—front or back—may only be possible by understanding the layered internal corneal anatomy. For example, the distinction between irregularities in the flap profile (keratome)—flap positioning (surgeon) vs the stromal bed (laser)—will aid in planning further surgical correction. In addition, further surgery on the cornea should always be based on a full knowledge of the remaining tissue available.

Below are several examples of cases within, and commonly referred to, our practice for Artemis anatomical evaluation after complicated LASIK in which Artemis provided essential information for further treatment planning.

Microfolds

The occurrence of microfolds in the LASIK flap is often a visually compromising complication. There have been numerous suggestions as to how to treat microfolds, but not all have been based on an anatomical diagnostic classification.

We have studied the anatomical morphology of microfolds while correlating the VHF digital ultrasound scans to clinical slit-lamp examination and functional impact on vision. Founded upon these studies, we have devised a classification system that is based on clinical management options. The Reinstein classification is shown in Table 3-1. Folds are initially classified as either involving the stromal component of the flap or Bowman's layer alone. If involving the stromal component of the flap, these are classified as flap corrugations, representing gross flap malposition that in effect lead to undulation and waviness of stromal lamellae within the entire flap substance. Flap corrugations must clearly be managed by flap lifting and repositioning. If the folds involve Bowman's layer, a distinction must be made between true microfolds and Bowman's cracks because their management is completely different. True microfolds are literally grooves in Bowman's layer (Figure 3-7) produced by redundancy due to flap malposition or incomplete distension. Bowman's cracks are fractures in Bowman's layer with no grooving (Figure 3-8). Bowman's cracks are caused by trauma to the flap that may result either from the stretching of

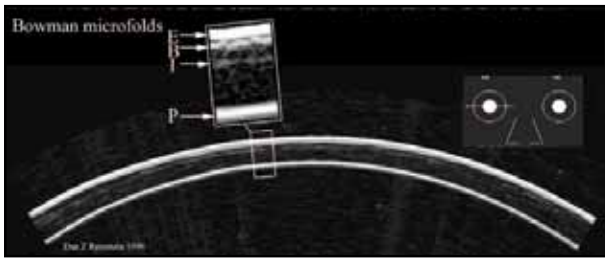


Figure 3-7. True Bowman's microfold. Horizontal VHF digital ultrasound corneal B-scan through the visual axis of a patient 6 months after LASIK. The surface of epithelium (E), Bowman's layer (B), the keratectomy interface (K), and the endothelium (P) are labeled. Inspection of the surface of Bowman's layer demonstrates a true microfold, with Bowman's layer showing a groove approximately 25 μm in depth and 100 μm in width.

Bowman's layer when dragging the flap from the hinge with a spatula or from folding or bending of Bowman's layer when returning the flap to the bed (especially if the flap has dried during the period of ablation). The distinction between true microfolds and Bowman's cracks is very important because while it may be warranted to relift a flap with true microfolds to adequately reposition the flap and distend the grooves to improve refraction and BSCVA, lifting a flap with Bowman's cracks will further traumatize the flap causing additional damage and potentially delaying the return of BSCVA.

Flap Complications

The postoperative assessment of flap complications is greatly aided by VHF digital ultrasound scanning. Determination of the exact anatomy of the faulty lamellar dissection will show at what depth the flap was created and whether flap repositioning was optimal. This information is important in the planning of a subsequent recutting of another flap. In addition, for cases with central flap dissections or irregularities, VHF digital ultrasound can determine if the edges of Bowman's layer were properly and adequately apposed in order to help avert epithelial ingrowth.

Buttonholed Flaps

In the following example, a 33-year-old nurse underwent LASIK in 1998 with the Moria LSK One and the Nidek EC5000 for a -5.50 sphere. The preoperative corneal thickness was 509 μm and the predicted residual stromal thickness was 280 μm (based on a 160- μm flap). Because she lived far away, we did not see her until almost 2 years later. She eventually presented in 1999 requesting that one of the eyes, which had regressed in the first 3 months after surgery, be enhanced. General opinion at

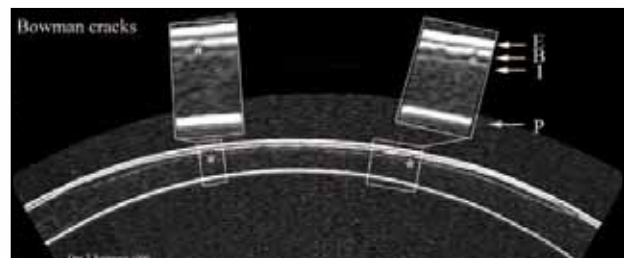


Figure 3-8. Bowman's cracks. Horizontal VHF digital ultrasound corneal B-scan through the visual axis of a patient 9 months after LASIK. The surface of epithelium (E), Bowman's layer (B), the keratectomy interface (K), and the endothelium (P) are labeled. Inspection of the Bowman's interface demonstrates fractures or discontinuities (*) that do not involve grooving or puckering of Bowman's layer.

the time dictated recutting flaps rather than lifting, ostensibly because flap lifting after 6 months was assumed to be difficult and recutting was assumed to lead to less chance of epithelial ingrowth due to the sharp edges of the new flap. The patient underwent recutting with the Hansatome using the 160- μm head and the 9.5-mm ring (aiming to go outside, but superficial to the original flap to save residual stromal tissue). The result was a central buttonhole within a double flap dissection, which was replaced without performing laser ablation. Figure 3-9 shows the exact anatomical result 1 day after flap replacement. From the ultrasound scans it was clear that the Hansatome flap had managed to stay superficial and within the original flap, only to then exit (Figure 3-9, X1) through Bowman's layer and epithelium and then re-enter (Figure 3-9, X2) the cornea to regain the plane superficial to the original flap interface. The scan reassured us that Bowman's layer was properly apposed and that anatomical restoration had been achieved for a good prognosis. At 2 years thereafter, she had not developed epithelial ingrowth and remained without loss of BSCVA.

Short Flaps

In 1994, we coined Reinstein's Law of Epithelial Compensation for irregular astigmatism³¹: "Irregular astigmatism results in irregular epithelium." The epithelium often compensates fully for stromal surface irregularities, keratoconus being an excellent example of this. Everyone knows that as cone formation in keratoconus progresses, the epithelium overlying the cone becomes progressively thinner. This is because the epithelium becomes invaginated by the underlying bulging stromal surface while its outer surface is kept as regular as possible by the action of 10,000 blinking events a day. In fact, this is why keratoconus can be detected earlier by looking at the back sur-

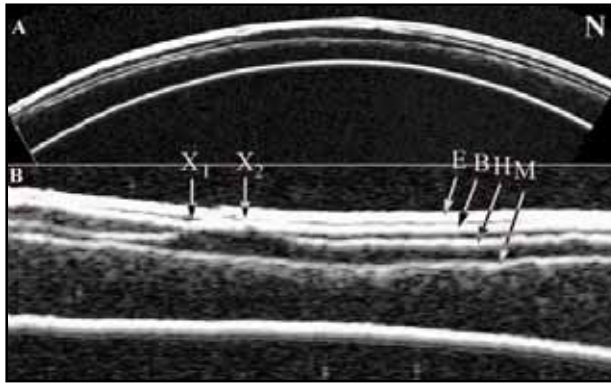


Figure 3-9. Geometrically corrected horizontal VHF digital ultrasound corneal B-scan of a cornea 1 day after recutting a second flap and obtaining a simultaneous separation of the original flap from the bed and a buttonhole (A). An axially zoomed image in a different horizontal plane is shown below (B). The surface of epithelium (E), Bowman's layer (B), the keratectomy produced by the second-cut Hansatome 160-head (H), and the original Moria keratectomy interface (M) are labeled. The Hansatome interface is seen to course superficially to the original keratectomy as intended from left to right, but superficializing, exiting through Bowman's (X1) and the epithelium, then re-entering the epithelium and crossing Bowman's (X2) to again find a plane superficial to the original keratectomy. Exact anatomical apposition of Bowman's is confirmed by the scan, thus confirming perfect flap repositioning and minimizing the probability of epithelial ingrowth in the visual axis.

face topography of the cornea rather than the front surface. We are investigating whether examination of epithelial thickness profiles may provide an even earlier and therefore more sensitive screening tool for keratoconus. According to Reinstein's Law of Epithelial Compensation, if a patient presents with stable irregular astigmatism, by definition the epithelium has reached its maximum compensatory function.

In the following example, a 23-year-old patient underwent LASIK in the left eye in 1998 using the Moria LSK One microkeratome in which a short, nasal-hinged flap was obtained and the laser ablation was performed. VHF digital ultrasound scanning is shown in Figure 3-10. A large amount of epithelial compensation takes place in cases like this in which there are large steps in the shape of the stromal surface. This is why neither topography-guided nor wavefront-guided ablations will be sufficient to correct such complications. In this case, the stromal surface is asymmetric. The epithelium has compensated as much as it can, but is still leaving asymmetry and the

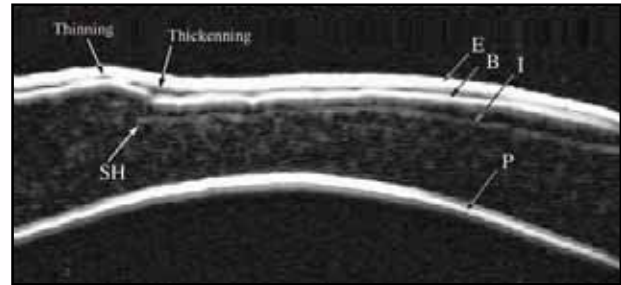


Figure 3-10. Horizontal VHF digital ultrasound corneal B-scan through the visual axis of the left cornea of a patient in whom a slightly short flap was created and the ablation was carried out. The surface of epithelium (E), Bowman's layer (B), the keratectomy interface (I), and the endothelium (P) are labeled. The abrupt termination of the keratectomy producing a short hinge is shown (SH). Lack of ablation nasal to this has produced a large step in the cornea. The stromal surface step is partially compensated for by epithelial remodeling; the epithelium characteristically thins over the "bump" while thickening in the crevice produced. This cross-section clearly demonstrates why topography-guided ablations (or even wavefront-guided ablations, which are 70% biased to the front surface) will not be fully successful in correcting the stromal irregularity.

patient presents with topographic asymmetric astigmatism. If one were to base the corrective ablation profile on the topography or ocular wavefront now (70% epithelial surface shape dependent), there would clearly be ineffective correction of the stromal surface shape. Following such a case, the epithelium may or may not compensate fully for the remaining stromal surface asymmetry. If it does, the topography would become regular but the patient may still have symptoms due to the significant refractive index difference between the epithelium and the stroma.¹¹

The Topographic Diagnosis of Decentration: Is It Really a Laser Decentration?

Decentration is a diagnosis made postoperatively by inspection of topography. Decentration denotes off-center ablation. We have found that what appears to be decentration by topography is not always due to off-center ablation.

In the following example, a patient presented to us complaining of monocular double vision after LASIK. The initial refraction was -6.50 D. Treatment was carried out with the Moria LSK One microkeratome and the Nidek EC5000. Preoperative corneal thickness by Orbscan was measured as 516 μm . With an ablation depth

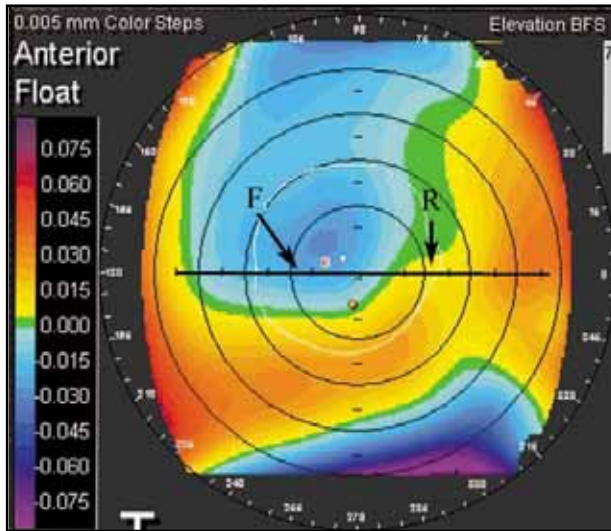


Figure 3-11. Orbiscan anterior best fit sphere (default 10-mm zone fit) plot of the cornea in a patient presenting with monocular diplopia and a topographic diagnosis of “decentered ablation” proved incorrect by B-scan imaging in the plane represented by the horizontal black line. Flatter (F) and raised (R) areas are correlated to the ultrasound B-scan in Figure 3-13.

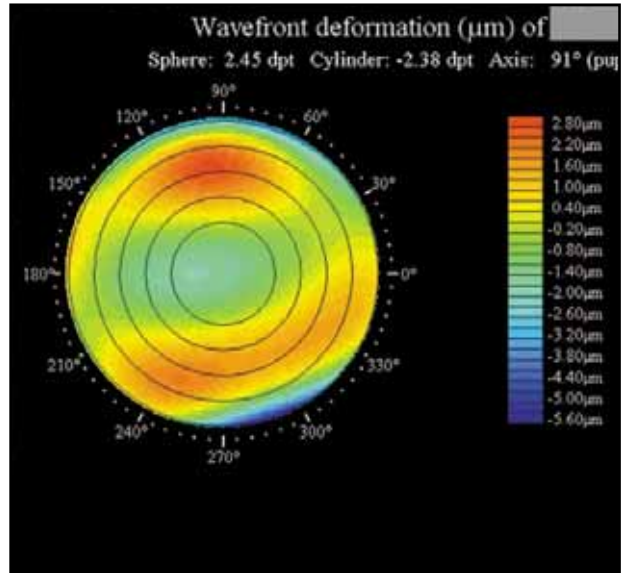


Figure 3-12. Zywave aberrometry displaying the high-order wavefront plot of the eye represented in Figure 3-11 of a patient presenting with monocular diplopia and a topographic diagnosis of “decentered ablation.” There is marked coma. Conventional wisdom would dictate ablation that would involve relatively more removal of tissue in the yellow-to-red zones. B-scan imaging (Figure 3-13) proves this to be inappropriate for this case.

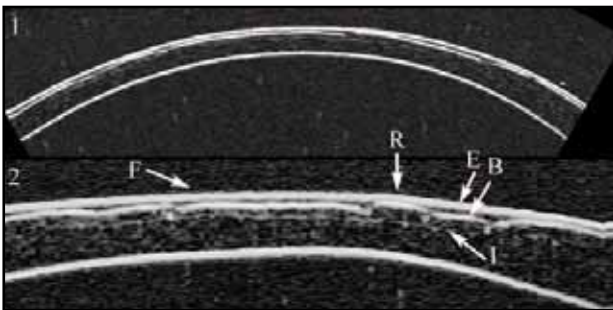
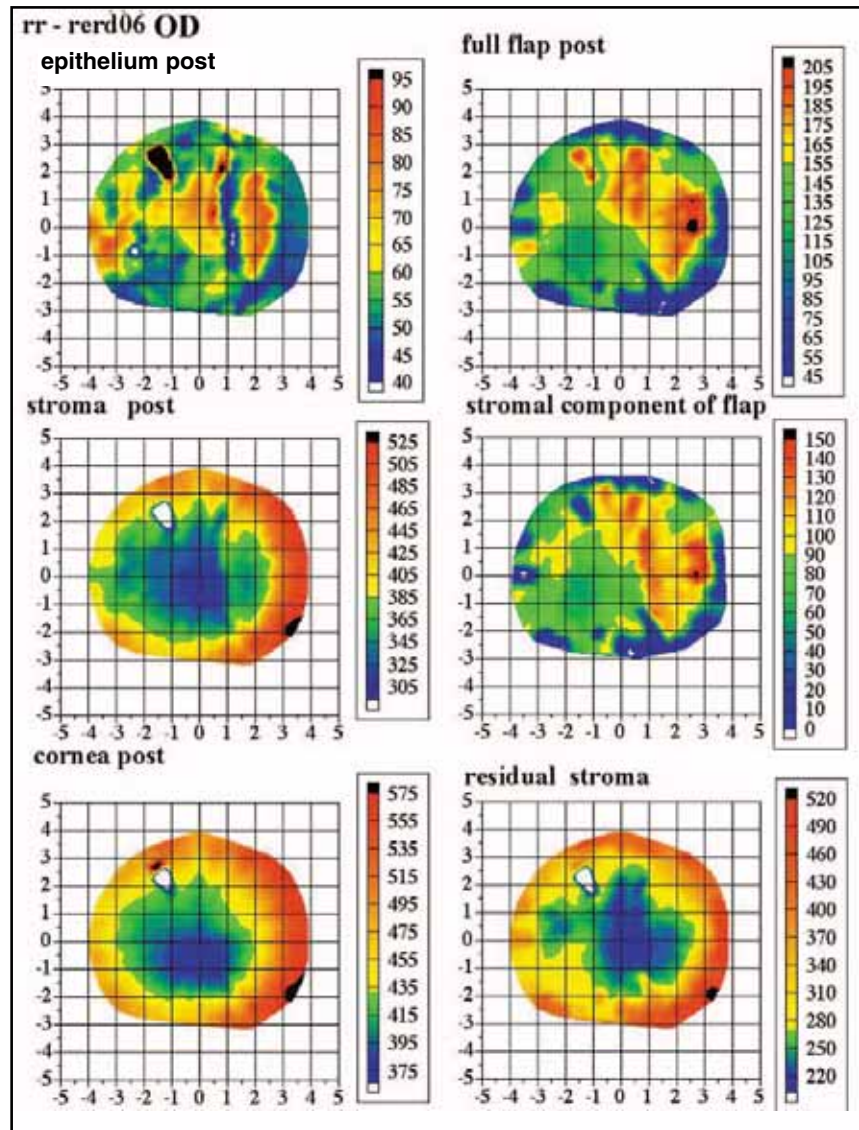


Figure 3-13. Horizontal VHF digital ultrasound corneal B-scan through the visual axis of the right cornea of a patient presenting with monocular diplopia and a topographic and wavefront diagnosis consistent with “decentered ablation.” The upper image (1) shows the geometrically corrected image, while the lower image (2) shows the raw ultrasound data with axial zoom to better appreciate the interfaces. The surface of epithelium (E), Bowman’s layer (B), and the keratectomy interface (I) are labeled. It is clearly noted that Bowman’s surface is highly irregular, with numerous true microfolds (*) that were only very faintly visible on slit-lamp examination due to the impressive epithelial compensation producing excellent smoothing of the corneal surface. The diagnosis of “decentered ablation” is clearly less likely than that of an inadequately distended flap, producing surface asymmetry. Appropriate management would most likely involve flap distension and repositioning, not further laser ablation.

of 90 µm, the predicted postoperative residual stromal thickness was 266 µm. On examination, his uncorrected visual acuity (UCVA) was 20/70; manifest refraction was +3.00 -3.75 x 96 yielding a BSCVA of 20/40+2. Slit-lamp examination showed a clear cornea with an unremarkable flap possessing a few very faint, faded shallow-appearing vertical microfolds. Orbiscan anterior best fit sphere mapping is shown in Figure 3-11, providing a differential diagnosis of decentration of the ablation zone, or ectasia. Figure 3-12 shows Zywave (Bausch & Lomb Surgical, Irvine, Calif) aberrometry of the same eye, demonstrating coma-like higher-order aberrations.

Horizontal 3-D VHF digital ultrasound B-scan cross-section of the cornea revealed anatomical features that provided further diagnostic information. Figure 3-13 shows the B-scan demonstrating a flatter (F) nasal side of the cornea, with a raised (R) surface temporally as found also on the Orbiscan best fit sphere surface shape map. Beneath the raised (R) area the epithelial thickness is seen to be reduced due to invagination by the underlying Bowman’s layer (B). Bowman’s layer (B) is highly irregular, showing three major ultrasonic discontinuities (*) representing either cracks or microfolds in the flap surface. Three-dimensional pachymetric topography of this

Figure 3-14. Reinstein “C6” corneal pachymetric map display of the thickness in microns (color scale) of the epithelium, stroma, full cornea, stromal component of the flap, and residual stromal bed in the case of monocular diplopia with a topographic diagnosis of “decentered ablation.” The residual stromal thickness minimum is 223 μm (second column, third row). Inspection of the epithelial thickness profile (first column, first row) demonstrates the error introduced by epithelial compensation if one were to attempt topography-guided or wavefront-guided ablation to correct the optical defect. B-scan imaging (Figure 3-13) confirms that laser ablation would be a less optimal management strategy in this case, in which there is extreme flap bunching due to inadequate distension.



cornea is shown in Figure 3-13. The epithelial thickness profile is seen to vary continuously, filling in and smoothing out the surface of Bowman’s layer. The thinnest point within the residual stromal bed, as determined by 3-D thickness mapping in a Reinstein C6 (post-LASIK with no preoperative data for subtraction maps) display (Figure 3-14) is 223 μm . The residual stromal layer thickness profile appears slightly asymmetric or decentered in the nasal direction. Inspection of the stromal component of the flap map (Figure 3-14, second column, second row) shows the reason for this: the stromal component of the flap was thicker temporally than nasally. The central stromal component of the flap was 80 μm , thus implying that the central flap thickness was originally approximately 130 μm (80+50). The original surgeon had calculated that the

patient would still have 266 μm under the flap after treatment. Given that this is 43 μm less than observed, and that the flap was 30 μm thinner than intended, it is probable that his preoperative pachymetry (by Orbscan) was underestimated by approximately 43 μm and that the original corneal thickness must have been closer to 473 μm .

A diagnosis was made of flap malposition and possible asymmetric biomechanical shift. In addition, the residual stromal thickness was noted to be too thin for further under-the-flap ablation, despite the fact that the preoperative parameters would have implied that there was room for further treatment.

This case clearly illustrates the importance of anatomical diagnosis as in contrast to a topographical description

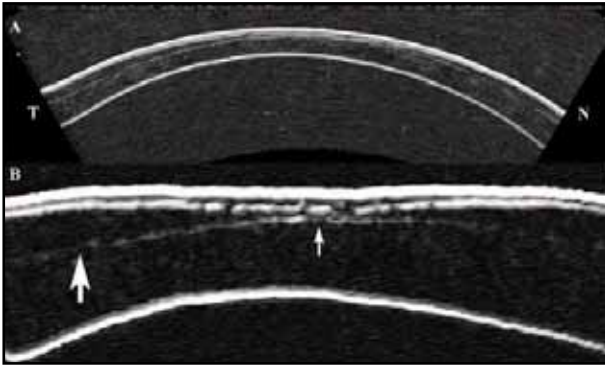


Figure 3-15. Horizontal VHF digital ultrasound B-scan through the visual axis of a cornea 3 months after LASIK for -10.00 which produced a gross overcorrection to +4.00 D. The geometrically correct image is shown above (A) with the raw scan data axially zoomed below (B). The flap is seen to be much thinner centrally (small arrow) than peripherally (large arrow). This unplanned, extreme, mid-peripheral, deep keratectomy explains the gross overcorrection. Central flattening occurred as a function of three mechanisms acting together: laser ablation, radial keratotomy-like peripheral bulging with central flattening, and Roberts'-like peripheral corneal thickening due to lamellar relaxation producing increased central flattening. Clearly, relifting of this flap and further midperipheral ablation (as would have been carried out before this diagnostic test) would risk exacerbating the hyperopic shift by further unpredicted biomechanical changes in the cornea.

in planning the management of the complications of LASIK. By topography alone, this case may well have been diagnosed as a decentration. The eye may well have then undergone a topographically guided treatment under the flap. Given the low residual stromal thickness, it is conceivable that further tissue removal would have led to further mechanical shifts, and an unpredictable result, with a high possibility of inducing progressive ectasia.³²

Flap Profile Irregularity

Flap profile irregularities can lead to irregular biomechanical shifts in refraction. A patient was able to undergo LASIK for the correction of -10.00 D oculus dexter (OD) because she had 5.5-mm scotopic pupils, and adequate corneal thickness to leave 250 μm in under an assumed 160- μm flap. The Moria CB microkeratome employing the “110” head, which is designed to cut an average of 140 μm was used in manual mode, with a deliberate “fast pass” of about 1 second in order to attempt to obtain a thinner flap. It was proposed that VHF digital ultrasound scanning would be used postoperatively to

measure flap and residual stromal thickness to decide if it would be possible to perform further enhancement if required. The procedure was uneventful, and the flap was intraoperatively noted to “feel” thin and to be of “good quality for a future flap-lift.” Day 1 postoperatively the refraction was +5.00 D with no loss of BSCVA. This only regressed to +4.00 D by 3 months. Figure 3-15 shows a horizontal cross-section of the flap 3 months after LASIK. It can be seen that the flap centrally was indeed thin; the stromal component of the flap was in the region of 90- to 100- μm thick. However, the stromal component of the flap reached over 200 μm peripherally (equating to an original flap thickness of over 250 μm). It is conceivable that this patient’s gross overcorrection was partly due to the following biomechanical causes:

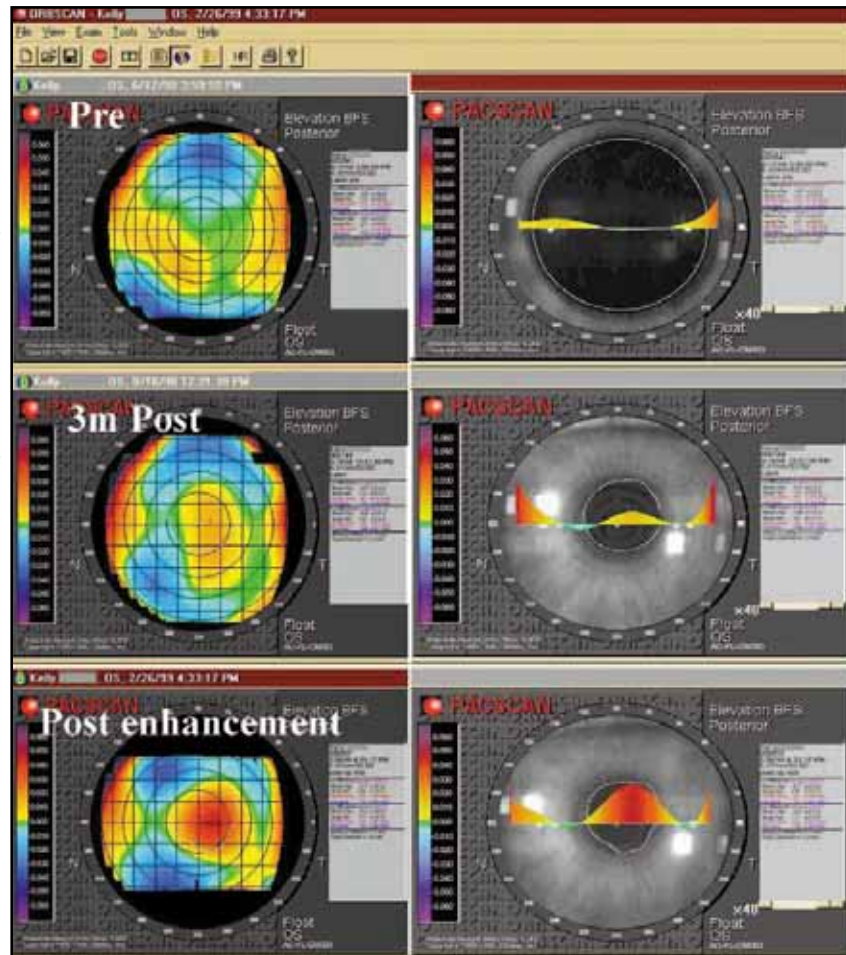
1. Deep keratectomy peripherally may have produced excess flattening centrally through a mechanism of peripheral thickening as proposed by Roberts¹⁹ combined with an effect similar to radial keratotomy.
2. Mid-peripheral bulging due to localized deep keratectomy causing central flattening. Clearly in this case a knowledge of the flap anatomy created will be essential in planning further treatment.
3. The relifting of the apparently good quality flap (as assessed intraoperatively) for hyperopic ablation to be performed would deepen the mid-peripheral keratectomy further, would probably not be ideal given the apparent mechanisms producing this excessive overcorrection.

Biomechanical Changes in the Cornea: Elastic vs Ectatic

Elastic changes in the cornea are comprised of forward or backward bending of the central cornea due to surgically induced lamellar structural changes, the influence of intraocular pressure, and other external forces to the cornea, but by definition should not be described as ectasia. Ectasia, as it relates to lamellar refractive surgery (and keratoconus, actually) should be defined according to the way it was done by the father of lamellar corneal refractive surgery: Jose Ignacio Barraquer-Moner. Barraquer defined ectasia as a progressive deformation of the cornea in which there is progressive corneal steepening and thinning.³³ As such, it describes a plastic and/or viscoelastic deformation.

In LASIK, it is important to determine the true anatomical diagnosis for secondary ametropia (ie, epithelial or biomechanical corneal changes), so that accurate cognitive surgical planning for enhancement surgery can be accomplished. Given the lack of consistency in flap thickness, when considering correction of secondary

Figure 3-16. Multiple Orbscan back surface best fit sphere plots before LASIK (first row), 3 months postoperatively (second row), and 6 months after enhancement (third row). The best fit sphere radius for all time stages are user set to the radius of the central 4-mm zone of the back surface before surgery (6.37 mm) to show back surface shifts in curvature relative to the preoperative state. The first column shows the 3-D maps, in 2-D, while the second column shows horizontal cross-sectional representation of the best fit to the initial 6.37-mm radius. At 3 months postoperatively, the back surface was seen to have decreased a little in radius relative to the preoperative state (relative bulging), and after enhancement, this back surface bowing is considerably increased.



ametropia (enhancement surgery) a knowledge of the whole RST bed is paramount for maximum safety. Currently, only the central RST is determined either from the assumed presurgical parameters or it is measured manually intraoperatively using a hand-held ultrasonic pachymeter.

In the following example, a 30-year-old woman underwent LASIK OS with the Nidek EC5000 and the Moria LSK One 130-head microkeratome in June 1998. The preoperative corneal thickness by Orbscan was 555 μm . The predicted ablation depth for correction of -6.25 -1.25 \times 175 (BSCVA 20/20) in a 6.5-mm zone was 101 μm , and the flap thickness used for predicting the residual stromal thickness was 160 μm . Therefore, the predicted residual stromal thickness was 293 μm ($555 - 101 - 160 = 293$). One week after treatment, the refraction was -1.00 -1.00 \times 170 and at 3 months, the refraction was -0.50 -1.75 \times 175 (BSCVA 20/20). Note that there was no correction of the original on-axis cylinder and an undercorrection of myopia. Given that there were 43 μm of residual stroma predicted still left over the 250 μm limit, an enhancement was performed lifting the original flap in

September 1998, using the Bausch & Lomb 217C (Irvine, Calif) (predicting a removal of a further 42 μm , bringing the predicted residual stromal thickness to a level of 251 μm). Intraoperative bed pachymetry (Sonogage II hand-held ultrasound pachymeter) measured 305 μm in the central bed under the flap before ablation of 42 μm as predicted by the laser. Six months following this enhancement, refraction was $+2.75$ -2.50 \times 90 (BSCVA 20/20) and the patient was complaining of double vision in that eye (even with best spectacle correction). There was a less than 100% overcorrection of on-axis cylinder. Given the fact that no further tissue was left under the flap for further treatment, it was decided to enhance it as a PRK over the original flap in April 1999 by what is now termed “advanced surface ablation” (ie, removal of the epithelium using 20% ethanol and ablation with the Bausch & Lomb 217C). The treatment performed was a positive cylinder ablation of plano $+2.50$ \times 180. Although the cornea remained clear and no haze developed, the refraction 6 months after this second enhancement was $+2.00$ -2.75 \times 175. Again, there was a greater than 100% over-

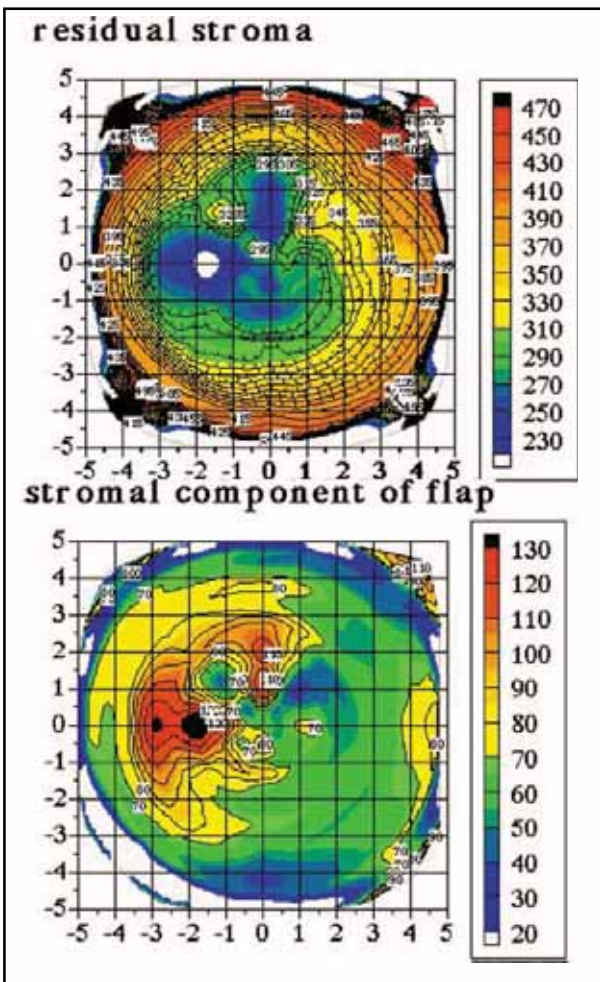


Figure 3-17. Three-dimensional pachymetric mapping of the residual stromal layer under the flap, and the stromal component of the flap (ie, excluding epithelium) created with a nasal hinge with the Moria LSK One using the 130 head. The central thickness of the stromal component of the flap is 65 μm , corresponding to an original flap thickness of approximately 115 μm (65 + 50). However, 2-mm nasal to the center of the flap the stromal component thickness was 139 μm , corresponding to an original flap thickness of 189 μm (139 + 50). This nasal increased thickness was responsible for an unpredictably low residual stromal thickness (above), which led initially to an unpredicted increase in cylinder in the horizontal plane, and subsequent unpredicted biomechanically based refractive shifts on repeated enhancement surgery.

correction of the cylinder and little change in the spherical equivalent.

The patient was referred to us for evaluation. We were able to obtain electronic files for all Orbscan examinations performed before and after surgery from her original

surgeon. After importing these into our Orbscan workstation, we displayed the best fit sphere back surface maps for preoperative, 3 months postoperative (pre-first enhancement), and 5 months postenhancement. All three back surface best spherical fit maps were exhibited side-by-side for comparison. We set the fit sphere curvature for all three time points to that of the preoperative back surface best fit sphere curvature of 6.37 mm as shown in Figure 3-16. The Orbscan back surface maps demonstrate how the central radius of curvature of the back surface decreased incrementally with each treatment. Why would this be occurring? More than 250 μm were predicted (and confirmed by intraoperative measurement) to have been left under the flap.

VHF digital ultrasound B-scanning was performed using the Cornell University arc scan prototype. Figure 3-17 shows the 3-D thickness map of the residual stromal layer, demonstrating a thickness centrally of approximately 270 μm , which was more than estimated by calculation based on preoperative parameters but close to what was predicted by the intraoperative pachymetry (305 – 42 = 263 μm). However, the RST 1.5-mm nasal to the center was found to be only 216 μm (the first enhancement under the flap would have reduced the thickness of the RST at this location by approximately 26 μm ; therefore, the RST here before the first enhancement was approximately 242 μm).

The cause of this RST bed asymmetry is evident from inspection of the thickness map of the stromal component of the flap. The stromal component of the flap 1.5 mm nasally was 139 μm compared to only 65 μm centrally. The original flap thickness nasally and centrally would have been 189 μm (139 + 50) and 115 μm (65 + 50), respectively. (Note: The PRK over the flap would not have removed some tissue from the nasal stromal component of the flap as it was a positive cylinder ablation).

The asymmetric flap thickness, with an RST below 250 μm in the nasal portion of the cornea may explain why this patient's cornea was behaving unpredictably on repeated enhancements. Reinstein et al have shown that significant and measurable biomechanical changes occur in the cornea after LASIK with a residual stromal thickness below 290 μm ,^{28,29} and this asymmetric RST bed may be responsible for unpredicted biomechanical shifts as evidenced by the serial back surface Orbscan exams shown in Figure 3-16.

Had VHF digital ultrasound scanning been performed before the first enhancement, it would have been evident that the RST was already below 250 μm nasal to the center after the first treatment. This may have alerted the surgeon to not lift the original flap and remove further tissue from under it, and may have avoided the eventual induction of biomechanically mediated asymmetric astigmatism with monocular diplopia.

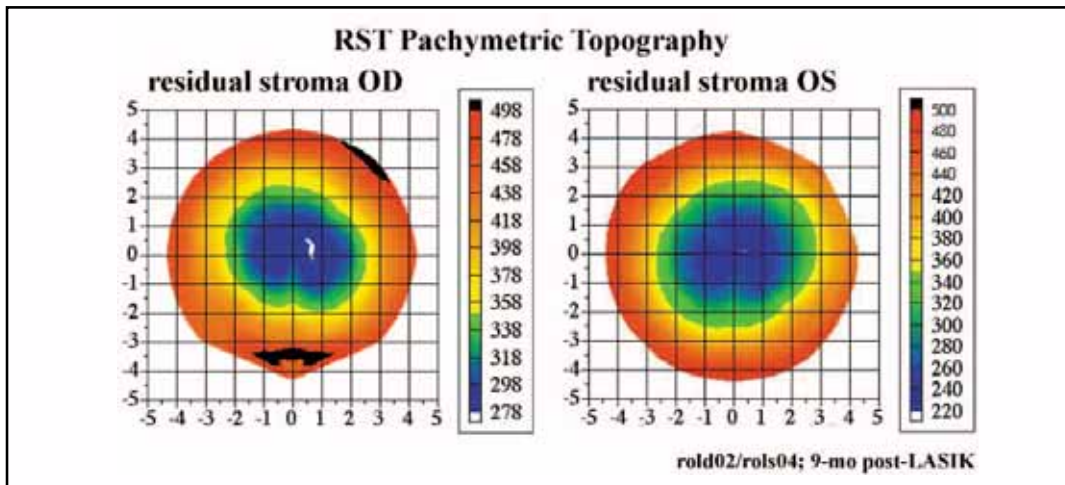


Figure 3-18. Three-dimensional residual stromal thickness maps of the right and left eyes of a patient who had undergone routine LASIK with predicted residual stromal thicknesses of 283 μm OD and 281 μm OS. As seen here, the thinnest points of the residual stromal beds were in fact 278 μm and 221 μm on the right and left, respectively, perhaps accounting for a slightly greater myopic undercorrection on the left due to a biomechanical corneal shift. The determination of this low residual stromal thickness on routine Artemis scanning prevented the removal of a further 20 μm that would have resulted in an RST of 201 μm , and probably a high risk of developing ectasia. Artemis scanning for verification of residual stromal thickness is a powerful tool for increasing the safety of enhancement surgery.

In another example, a 33-year-old female underwent simultaneous bilateral LASIK (OS first, OD second) in May 2002 for $-6.00 -0.50 \times 115$ (20/15) OD and $-6.00 -0.50 \times 20$ (20/15) OS. Treatment was carried out with the Hansatome 160- μm head, and the MEL70 excimer laser with ablation depths of 99 μm for each eye (6.5-mm fully corrected optical zone). Preoperative Orbscan thicknesses were 542 μm OD and 540 μm OS, yielding predicted RST of 283 μm OD and 281 μm OS. UCVA was 20/15-2 in both eyes at 1 month. Refractions were plano -0.50×125 OD and -0.50D OS. In February 2003, 9 months postoperative, UCVA was 20/25 OD and 20/30 OS and refraction was $-0.50 -0.50 \times 150$ (20/15) OD and $-0.75 -0.25 \times 145$ (20/15) OS. As per enhancement protocol in our practice, she underwent Artemis scanning for determination of the RST before enhancement. RST maps for right and left eyes are shown in Figure 3-18. The minimum RST was 278 μm OD and 221 μm OS. Central thickness of the stromal component of the flap was 85 μm OD and 135 μm OS, corresponding to original flap thicknesses of 135 μm OD and 185 μm OS. We reported VHF digital ultrasound pachymetric mapping of Hansatome flaps created bilaterally using the same blade. The mean (\pm SD) central thickness for first eyes was 139 (\pm 21.3) μm and second eyes was 122 (\pm 22.4) μm . Second flaps were statistically significantly thinner than first flaps.³⁴ Therefore, it is not surprising that the right flap was thinner than the left. However, the left (first) flap was approx-

imately 15 μm thicker than expected (185 vs 160). Since the RST was 60 μm thinner than expected, it can be concluded that the Orbscan preoperatively overestimated corneal thickness by approximately 45 μm (originally predicted RST – flap thickness over 160 – RST achieved = 281 – 15 = 221). Therefore, in this case, RST monitoring by direct measurement before what appeared to be a relatively benign enhancement, with adequate tissue reserve, resulted in removing excess tissue from the bed of a cornea already biomechanically compromised with an RST of 221 μm . Had ablation been carried out for the enhancement under the flap, assuming a residual of 283 μm as predicted, ablation in a 7-mm zone of 20 μm would have reduced the RST to approximately 201 μm , with the surgeon assuming that there was still 263 μm of RST. Conceivably, this would have led to further biomechanical change and a myopic shift,²⁸ possibly a second enhancement and the risk of inducing ectasia³² with the surgeon believing that more than 250 μm were being left under the original flap. In fact, many current publications on biomechanical changes and ectasia in the cornea after LASIK are based on the predicted value for the RST based on preoperative parameters.³⁵⁻³⁷ Our mathematical modeling using VHF digital ultrasound-based direct measurement of the RST lead us to determine that ectasia probably occurs on the average at an RST of 180 μm .³² We have studied the relative predictability of the RST in LASIK and found that with modern pachymetry

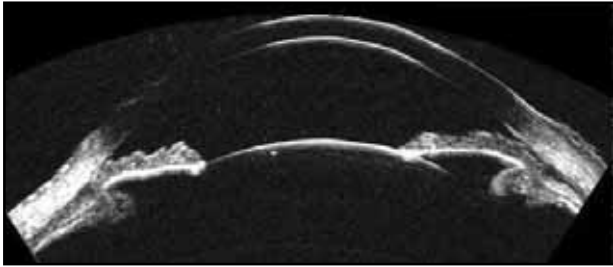


Figure 3-19. Full anterior segment horizontal VHF digital ultrasound B-scan encompassing a 15-mm wide sector. The anterior retina can be seen within this scan plane also. The angle-to-angle and sulcus-to-sulcus diameters are easily measured directly. Anterior chamber and posterior chamber volume and dimensions can be studied before insertion of phakic IOLs to predict the separation of such implants from the endothelium of the cornea, or the crystalline lens. Predictive effects on the angle due to posterior chamber phakic IOLs could also be made prospectively to improve patient safety.

(Orbscan and hand-held ultrasound pachymetry), microkeratome, and laser ablation depths, the RST can be predicted within a standard deviation of $30\ \mu\text{m}$ ³⁸ and hence a range of approximately $\pm 45\ \mu\text{m}$ (95% confidence interval). It is therefore prudent to stay within the Barraquer rule of aiming to leave $250\ \mu\text{m}$ under a lamellar flap³³ in order to avoid breaching this $180\text{-}\mu\text{m}$ limit.

Given our experience in the subject, our current thinking is that ectasia will occur if either less than $200\ \mu\text{m}$ are left under the flap or if LASIK is performed in a cornea with undiagnosed keratoconus. Therefore, accurate biometry before LASIK, after LASIK, and before enhancement, as well as cross-interpretation with Orbscan front and back surface shape evaluation, should protect all corneas from ectasia, with the exception of those that harbor undiagnosed (or unexpressed) keratoconus.

A NOTE ON PHAKIC INTRAOCULAR LENS SURGERY

There are currently no phakic intraocular lenses (IOLs) approved by the US Food and Drug Administration (FDA), and this is almost certainly contingent (for angle-supported and posterior chamber lenses) on the lack of adequate preoperative internal ocular biometry in surgical planning. Maximizing the safety of phakic IOLs is the honourous responsibility of surgeons who expect these devices to remain in normal eyes for several decades without causing serious side effects.

One of the most unique contributions to ophthalmology by the Artemis 2 will be in the sizing of IOLs, particularly phakic IOLs. Incorrect lens sizing or positioning can lead to long-term complications. One of the main safety hurdles encountered in anterior chamber, angle-supported phakic IOL implantation has been defining the correct amount of haptic force in the angle. If the lens is too large, this can lead to ischemia of the iris, causing iris stromal scarring and pupil ovalization. If too small, the lens may become displaced in the anterior chamber, risking endothelial damage or decreasing the ability to correct astigmatism with toric lenses. Issues relating to the sizing of posterior chamber lenses exist as well. If the vault of such a lens in the posterior chamber is too large, it can lead to narrowing of the anterior chamber angle. It can also increase the chances of pigment dispersion from the pigment epithelium of the iris with subsequent glaucomatous consequences. If the posterior chamber phakic IOL is too small, excessive contact between it and the crystalline lens may decrease aqueous flow and lens nutrition, as well as directly traumatize the lens surface, leading to cataract.

By providing accurate sulcus-to-sulcus and angle-to-angle measurements, the Artemis 2 has the potential to increase the safety of both anterior and posterior chamber phakic IOLs by improving the accuracy of lens sizing—a crucial issue for long-term safety of these devices (Figure 3-19). Until recently, surgeons have been using the external white-to-white measurement to estimate the internal, sulcus-to-sulcus, or angle-to-angle diameters.^{39,40} A recent study revealed either none or insufficient statistical correlation between the external ocular measurements (including white-to-white) and the internal angle-to-angle or sulcus-to-sulcus measurements of the eye, even if other conventional measurements (such as sphere, axial length, anterior chamber depth) were included.⁹ This means that the only alternative for ensuring the greatest sizing safety in phakic IOL surgery will be to determine angle-to-angle and sulcus-to-sulcus dimensions by direct measurement. To date, the Artemis 2 is the only technology available that can provide both these measurements directly, in 3-D, and under direct visualization for positional confirmation of the location from which measurements are taken. Without this feature, it would be relatively easy to measure internal ocular dimensions in the wrong plane (Figure 3-20).

Improving the safety of phakic IOLs by accurate anatomical surgical planning and postoperative monitoring could position phakic IOLs as a real alternative treatment for correcting lower refractive errors where extraocular corneal refractive surgery is the first-line approach currently.

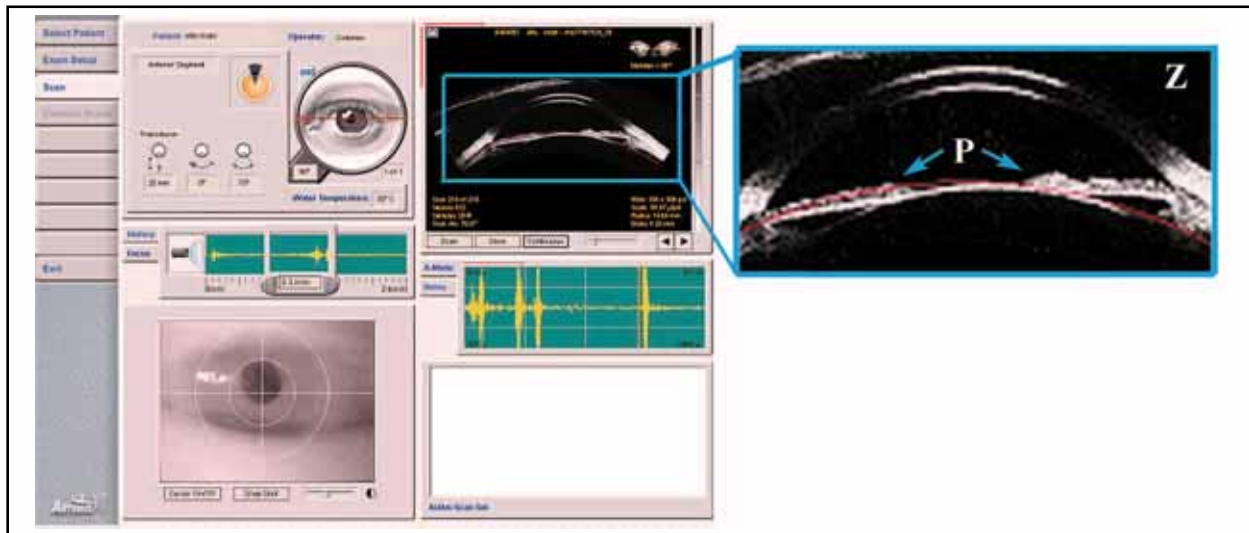


Figure 3-20. Screen capture from the Artemis during an anterior segment patient exam for direct measurement of the sulcus-to-sulcus. Real-time horizontal B-scans are displayed on the upper right quadrant of the screen. The infrared simultaneous video image shows that the position of the horizontal scanning plane is not central or axial. The zoom window (Z) of the B-scan shows a cross-sectional anterior segment representation containing pupil borders (P) that, in the absence of positional information, could have been interpreted as an axial scan, producing a false low sulcus-to-sulcus diameter. Similarly the angle-to-angle would have been underestimated falsely. Simultaneous video control is paramount for maximizing the safety of phakic IOL sizing, as improper localization will lead to erroneous biometry and the potential for oversizing of phakic IOLs.

CONCLUSION

Orthopedic surgery was practiced without pre- and postoperative anatomical imaging until the discovery of X-ray imaging in 1895 by Wilhelm Konrad Roentgen. Perhaps layer-by-layer anatomical imaging and biometry of the cornea and anterior segment will have a similar impact on refractive surgery.

REFERENCES

- Pavlin CJ, Sherar MD, Foster FS. Subsurface ultrasound microscopic imaging of the intact eye. *Ophthalmology*. 1990;97(2):244-250.
- Cusumano A, Reinstein DZ, Silverman RH, Belmont S, Coleman DJ. Very high-frequency ultrasound analysis of lamellar corneal refractive procedures. *Invest Ophthalmol Vis Sci*. 1997;34(4):S698.
- Coleman DJ, Woods S, Rondeau MJ, Silverman RH. Ophthalmic ultrasonography. *Radiol Clin North Am*. 1992;30(5):1105-1114.
- Reinstein DZ, Silverman RH, Coleman DJ. High-frequency ultrasound measurement of the thickness of the corneal epithelium. *Refract Corneal Surg*. 1993;9(5):385-387.
- Reinstein DZ, Silverman RH, Trokel SL, Coleman DJ. Corneal pachymetric topography. *Ophthalmology*. 1994;101(3):432-438.
- Reinstein DZ, Silverman RH, Rondeau MJ, Coleman DJ. Epithelial and corneal thickness measurements by high-frequency ultrasound digital signal processing. *Ophthalmology*. 1994;101(1):140-146.
- Reinstein DZ, Silverman RH, Sutton HF, Coleman DJ. Very high-frequency ultrasound corneal analysis identifies anatomic correlates of optical complications of lamellar refractive surgery: anatomic diagnosis in lamellar surgery. *Ophthalmology*. 1999;106(3):474-482.
- Reinstein DZ, Silverman RH, Raevsky T, et al. A new arc-scanning very high-frequency ultrasound system for 3D pachymetric mapping of corneal epithelium, lamellar flap and residual stromal layer in laser in situ keratomileusis. *J Refract Surg*. 2000;16:414-430.
- Reinstein DZ, Silverman RH, Lloyd OH. Estimation of angle-to-angle or sulcus-to-sulcus from white-to-white and conventional ocular measurements: are there adequate correlations for safe phakic-IOL surgery? Paper presented at European Society of Cataract and Refractive Surgery Annual Meeting; September 7-11, 2002; Nice, France.
- Reinstein DZ, Aslanides IM, Patel S, et al. Epithelial lenticular types of human cornea: classification and analysis of influence on PRK. *Ophthalmology*. 1995; 102(suppl):156.
- Patel S, Reinstein DZ, Silverman RH, Coleman DJ. The shape of Bowman's layer in the human cornea. *J Refract Surg*. 1998;14(6):636-640.

12. Reinstein DZ, Polack PJ, McCormick S, Rondeau MJ, Coleman DJ. High frequency ultrasound scanning of corneal scar formation in vivo. *Invest Ophthalmol Vis Sci.* 1992;33(4):1233.
13. Reinstein DZ, Silverman RH, Trokel SL, Allemann N, Coleman DJ. High-frequency ultrasound digital signal processing for biometry of the cornea in planning phototherapeutic keratectomy. *Arch Ophthalmol.* 1993;111(4):430-431.
14. Aslanides IM, Reinstein DZ, Silverman RH, et al. High-frequency ultrasound spectral parameter imaging of anterior corneal scars. *CLAO J.* 1995;21(4):268-272.
15. Allemann N, Chamon W, Silverman RH, et al. High-frequency ultrasound quantitative analyses of corneal scarring following excimer laser keratectomy. *Arch Ophthalmol.* 1993;111(7):968-973.
16. Lazzaro DR, Aslanides IM, Belmont SC, et al. High frequency ultrasound evaluation of radial keratotomy incisions. *J Cataract Refract Surg.* 1995;21(4):398-401.
17. Silverman RH, Reinstein DZ, Raevsky T, Coleman DJ. Improved system for sonographic imaging and biometry of the cornea. *J Ultrasound Med.* 1997;16(2):117-124.
18. Reinstein DZ, Sutton HFS, Srivannaboon S, Silverman RH, Coleman DJ. Microkeratome efficacy: 3D thickness assessment of corneal lamellar flap accuracy and reproducibility by arc-scanning very high-frequency digital ultrasound. *J Refract Surg.* In press.
19. Roberts C. The cornea is not a piece of plastic. *J Refract Surg.* 2000;16(4):407-413.
20. Holland SP, Srivannaboon S, Reinstein DZ. Avoiding serious corneal complications of laser assisted in situ keratomileusis and photorefractive keratectomy. *Ophthalmology.* 2000;107(4):640-652.
21. Boscia F, La Tegola MG, Alessio G, Sborgia C. Accuracy of Orbscan optical pachymetry in corneas with haze. *J Cataract Refract Surg.* 2002;28(2):253-258.
22. Prisant O, Calderon N, Chastang P, Gatinel D, Hoang-Xuan T. Reliability of pachymetric measurements using Orbscan after excimer refractive surgery. *Ophthalmology.* 2003;110(3):511-515.
23. Iskander NG, Anderson Penno E, Peters NT, Gimbel HV, Ferensowicz M. Accuracy of Orbscan pachymetry measurements and DHG ultrasound pachymetry in primary laser in situ keratomileusis and LASIK enhancement procedures. *J Cataract Refract Surg.* 2001;27(5):681-685.
24. Patel S, Alio JL, Perez-Santonja JJ. A model to explain the difference between changes in refraction and central ocular surface power after laser in situ keratomileusis. *J Refract Surg.* 2000;16(3):330-335.
25. Gauthier CA, Holden BA, Epstein D, Tengroth B, Fagerholm P, Hamberg-Nystrom H. Factors affecting epithelial hyperplasia after photorefractive keratectomy. *J Cataract Refract Surg.* 1997;23(7):1042-1050.
26. Lohmann CP, Reischl U, Marshall J. Regression and epithelial hyperplasia after myopic photorefractive keratectomy in a human cornea. *J Cataract Refract Surg.* 1999;25(5):712-715.
27. Srivannaboon S, Reinstein DZ, Sutton HFS, Silverman RH, Coleman DJ. Effect of epithelial changes on refractive outcome in LASIK. *Invest Ophthalmol Vis Sci.* 1999;40:S896.
28. Reinstein DZ, Srivannaboon S, Silverman RH, Coleman DJ. Limits of wavefront customized ablation: biomechanical and epithelial factors. *Invest Ophthalmol Vis Sci.* 2002;43:E-Abstract 3942.
29. Reinstein DZ, Srivannaboon S, Silverman RH, Coleman DJ. The accuracy of routine LASIK; isolation of biomechanical and epithelial factors. *Invest Ophthalmol Vis Sci.* 2000;2000:S318.
30. Patel S, Marshall J, Fitzke FW. Refractive index of the human corneal epithelium and stroma. *J Refract Surg.* 1995;11(2):100-105.
31. Reinstein DZ, Aslanides IM, Silverman RH, et al. Epithelial and corneal 3D ultrasound pachymetric topography postexcimer laser surgery. *Invest Ophthalmol Vis Sci.* 1994;35(4):1739.
32. Reinstein DZ, Srivannaboon S, Sutton HFS, Silverman RH, Shaikh A, Coleman DJ. Risk of ectasia in LASIK: revised safety criteria. *Invest Ophthalmol Vis Sci.* 1999;40(suppl):S403.
33. Barraquer JL. Queratomileusis y Queratofakia. Bogota: Instituto Barraquer de America; 1980.
34. Srivannaboon S, Reinstein DZ, Sutton HFS, Shaikh A, Silverman RH, Coleman DJ. Hansatome flap consistency analysis by 3D VHF ultrasound pachymetric topography. *Invest Ophthalmol Vis Sci.* 1999;40(4).
35. Seitz B, Torres F, Langenbucher A, Behrens A, Suarez E. Posterior corneal curvature changes after myopic laser in situ keratomileusis. *Ophthalmology.* 2001;108(4):666-672; discussion 73.
36. Pallikaris IG, Kymionis GD, Astyrakakis NI. Corneal ectasia induced by laser in situ keratomileusis. *J Cataract Refract Surg.* 2001;27(11):1796-1802.
37. Seiler T, Koufala K, Richter G. Iatrogenic keratectasia after laser in situ keratomileusis. *J Refract Surg.* 1998;14(3):312-317.
38. Reinstein DZ, Cremonesi E. Ectasia in routine LASIK: occurrence rate is reduced by one third when consistently using a thinner flap. *Invest Ophthalmol Vis Sci.* 2001;42(4):S725.
39. Zaldivar R, Oscherow S, Ricur G. The STAAR posterior chamber phakic intraocular lens. *Int Ophthalmol Clin.* 2000;40(3):237-244.
40. Baikoff G. Intraocular phakic implants in the anterior chamber. *Int Ophthalmol Clin.* 2000;40(3):223-235.